Journal of Power Sources 247 (2014) 539–544

Contents lists available at ScienceDirect

Journal of Power Sources

journal homepage: www.elsevier.com/locate/jpowsour

Short communication

Sensorless battery temperature measurements based on electrochemical impedance spectroscopy

L.H.J. Raijmakers [a], D.L. Danilov [a], J.P.M. van Lammeren [b], M.J.G. Lammers [b], P.H.L. Notten [a, *]

[a] Energy Materials and Devices (EMD), Department of Chemical Engineering and Chemistry, Eindhoven University of Technology, Den Dolech 2, 5600 MB Eindhoven, The Netherlands
[b] NXP Semiconductors, PO Box 80073, 5600 KA Eindhoven, The Netherlands

HIGHLIGHTS

- A new method is proposed to measure the internal temperature of (Li-ion) batteries.
- The temperature measurement is based on electrochemical impedance spectroscopy.
- The intercept frequency can be linked to the internal battery temperature.
- No hardware temperature sensors are required and heat transfer delay is absent.

ARTICLE INFO

Article history:
Received 29 June 2013
Received in revised form
13 August 2013
Accepted 2 September 2013
Available online 11 September 2013

Keywords:
Lithium ion battery
Intercept frequency
Internal battery temperature
Electrochemical impedance spectroscopy
Sensorless temperature measurement

ABSTRACT

A new method is proposed to measure the internal temperature of (Li-ion) batteries. Based on electrochemical impedance spectroscopy measurements, an intercept frequency (f_0) can be determined which is exclusively related to the internal battery temperature. The intercept frequency is defined as the frequency at which the imaginary part of the impedance is zero ($Z_{im} = 0$), i.e. where the phase shift between the battery current and voltage is absent. The advantage of the proposed method is twofold: (i) no hardware temperature sensors are required anymore to monitor the battery temperature and (ii) the method does not suffer from heat transfer delays. Mathematical analysis of the equivalent electrical-circuit, representing the battery performance, confirms that the intercept frequency decreases with rising temperatures. Impedance measurements on rechargeable Li-ion cells of various chemistries were conducted to verify the proposed method. These experiments reveal that the intercept frequency is clearly dependent on the temperature and does not depend on State-of-Charge (SoC) and aging. These impedance-based sensorless temperature measurements are therefore simple and convenient for application in a wide range of stationary, mobile and high-power devices, such as hybrid- and full electric vehicles.

1. Introduction

Li-ion batteries are nowadays the technology of choice to supply portable and mobile electronic devices with electrical energy. This can mainly be attributed to their ability to combine a high gravimetric/volumetric energy and power density, which leads to compact and low-weight batteries [1]. Since the 90s, Li-ion batteries have come to dominate small-scale applications such as portable phones and laptops. However, the breakthrough in large-scale applications such as (Hybrid) Electrical Vehicles was laborious, which is mainly caused by the high initial cost and safety issues [2]. To guarantee full safety, the automotive industry has established requirements and regulations in terms of security and reliability. Safety for batteries (packs) is strongly related to the temperature. When the temperature becomes too high, the battery can catch fire or even explode. For the success of the electric vehicle market this would be detrimental, if not fatal [3]. It is thus of high importance to have a reliable on-board thermal management system with proper temperature gauging.

Surface mounted thermal sensors like thermistors or thermocouples suffer from heat transfer delay due to the thermal mass of batteries (packs). Therefore, if the system is not in thermal

* Corresponding author. Tel.: +31 (0)40 247 3069.
E-mail address: p.h.l.notten@tue.nl (P.H.L. Notten).

0378-7753/$ – see front matter © 2013 Elsevier B.V. All rights reserved.
http://dx.doi.org/10.1016/j.jpowsour.2013.09.005

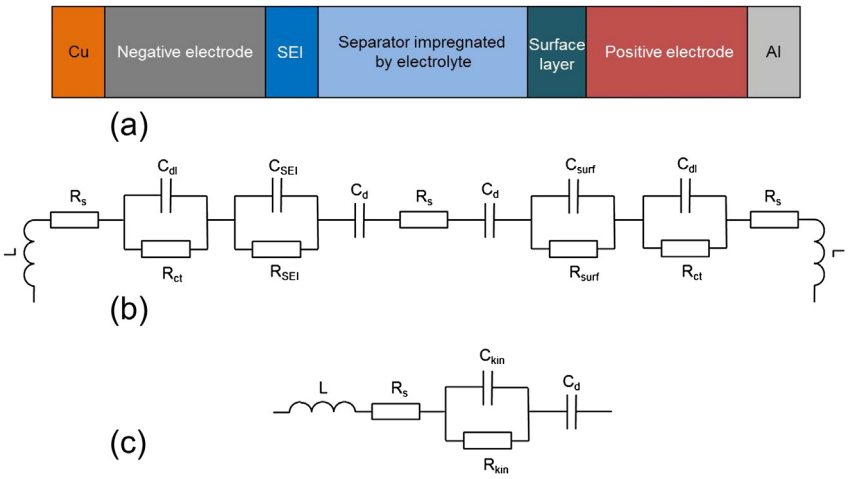

Fig. 1. (a) Schematic representation of a Li-ion battery; (b) Comprehensive equivalent circuit; (c) Simplified equivalent circuit.

equilibrium, the internal battery temperature differs from that externally. The internal temperature can forecast the risk of venting and thermal runaway, which might lead to spontaneous combustion [4]. It can also be used as measurement input for (thermal) Battery Management Systems. Forgez et al. [5] measured the internal battery temperature using a thermocouple to validate their model and to determine model parameters. A thermocouple was inserted in the center of a commercial cell by drilling a hole into the battery. This is, however, not a suitable approach for mass production. Lee et al. [6] developed a flexible micro-temperature sensor to *in-situ* monitor the temperature. Obviously, the disadvantage of this method is that a piece of hardware must be placed inside the battery.

Methods based on Electrochemical Impedance Spectroscopy (EIS) do not suffer from these disadvantages. EIS is a non-destructive technique designed to understand the operation of electrochemical systems [7]. It applies a harmonic voltage/current signal to the battery and analyzes the respective current/voltage response at various frequencies. After performing EIS, various diagnostic plots can be made. In particular, Nyquist plots are very instructive and may reveal a sloping line at low frequencies, a number of (depressed) semicircles at mid frequencies, and a vertical line at high frequencies. Although a lot of research has already been conducted, the exact identification of which process is responsible for a specific part of the spectrum is not trivial [8–10]. It is generally accepted that the high frequency semicircle can be attributed to the surface layer on the active electrode material [11–18] and that the mid-frequency semicircle can be attributed to the electrical double layer and electrochemical charge transfer reaction, occurring at the electrode/electrolyte interface [11,12,14–18]. Sloping lines are generally attributed to diffusion processes. It has been reported that the high frequency semicircle of commercial Li-ion cells is almost independent of SoC [9,12,14] whereas the temperature has a large influence [9,12,14].

In the high frequency region the impedance of a battery is generally dominated by its inductive behavior. This has been attributed to the porosity of the electrodes [19], the electrode geometry of spirally wound cells [20] or the conductive path formed by the terminals, connectors and electrodes [21–23]. As the porosity and electrode geometry hardly change upon cycling, the inductance is expected to remain more or less constant [10]. The inductance of commercial Li-ion batteries was found to be independent of SoC [14] and temperature [9,14]. The intercept frequency was also reported to be independent of both SoC and aging of Li-ion batteries [24,25]. Although it is known from literature that the intercept frequency changes as function of temperature [9] and is independent of SoC and aging, the relation between these has never been investigated in detail.

In this paper we extend on our earlier work [26], in which we introduce the concept of gauging the temperature by measuring the intercept frequency. The intercept frequency is defined as the frequency at which the Nyquist plot intersects the real axis. In other words, the intercept frequency is the frequency (f_0 [Hz]) or angular frequency ($\omega_0 = 2\pi f_0$ [rad s^{-1}]), at which the phase shift between voltage and current is zero. The intercept frequency can be measured by straightforward four-point impedance measurements. The advantage of measuring at the relatively high intercept frequencies is that these impedance measurements are less sensitive to variations in battery load currents. This is due to the fact that the intercept frequency is beyond the frequency range where the main electrochemical storage reactions of batteries take place. This makes it easier to perform accurate measurements even in systems under operation, such as driving electric vehicles.

2. Theoretical background

A schematic representation of a Li-ion battery is shown in Fig. 1a. Such a battery consists of two electrodes which are attached to a current collector (Cu and Al in the case of Li-ion) and are separated by a separator which is impregnated by a Li-salt containing electrolyte. It is generally considered that a Solid Electrolyte Interface (SEI) is formed at the surface of the negative and a surface film at the positive electrode. All these layers contribute to the overall battery impedance. A comprehensive equivalent electric network model can be constructed, as shown in Fig. 1b, to simulate the overall impedance where L represents the inductances and R_s the ohmic series resistances of the connections, electrodes, electrolyte, and separator. The outer parallel capacitors and resistors represent the electrical double layer capacitance (C_{dl}) and the charge transfer resistance (R_{ct}) of the positive and negative electrode, respectively. Two more RC-elements represent the impedance of the (SEI) surface layers. The individual capacitors (C_d) are added to model diffusion in both electrodes. This detailed circuit is rather complicated for an analytical analysis and is, therefore, reduced to the circuit shown in Fig. 1c. In this reduced circuit a single RC-chain is combined with an inductance, a series resistance and a diffusion capacitance. This single RC-chain, comprising R_{kin} and C_{kin}, describes the combined charge transfer kinetics, double layer capacitances and surface layer behavior of both electrodes.

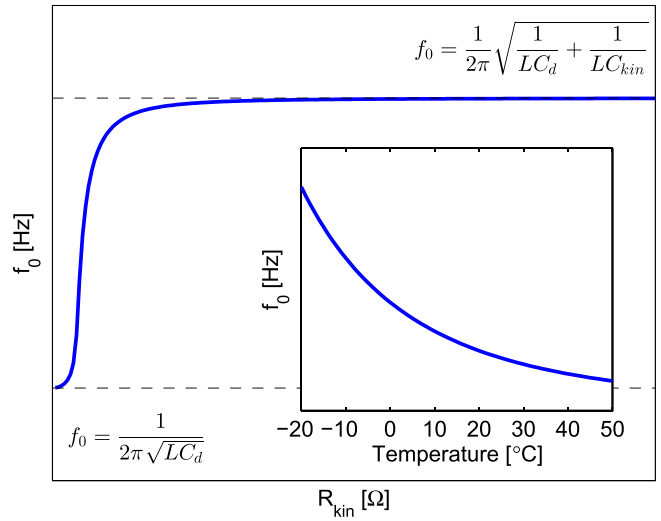

Fig. 2. Intercept frequency as a function of R_{kin} with the upper and lower limits (dashed lines) mathematically derived from Eq. (5). Insert: theoretical dependence of f_0 as a function of temperature. C_d = 1 F, C_{kin} = 0.01 F, L = 7 nH, $0 \le R_{kin} \le 0.02$ Ω, A = 400,000 Ω^{-1}, E_a = 10 kJ mol^{-1}, R = 8.314 J mol^{-1} K^{-1}, $253 \le T \le 323$ K.

The impedance of the equivalent circuit shown in Fig. 1c can easily be derived from the impedances of the separate elements, according to

$$Z_R = R,\ Z_C = \frac{1}{j\omega C},\ Z_L = j\omega L. \tag{1}$$

The total battery impedance (Z_b) is then given by

$$Z_b = j\omega L + R_s + \frac{1}{j\omega C_{kin} + \frac{1}{R_{kin}}} + \frac{1}{j\omega C_d}. \tag{2}$$

The imaginary part of Eq. (2) is calculated as

$$Z_{im} = \omega L - \frac{(C_{kin} + C_d)C_{kin}R_{kin}^2\omega^2 + 1}{C_d\omega\left(C_{kin}^2R_{kin}^2\omega^2 + 1\right)}. \tag{3}$$

The intercept frequency ω_0 can be calculated by equating Eq. (3) to zero. This results in the following bi-quadratic equation

$$C_dL\omega_0^2\left(C_{kin}^2R_{kin}^2\omega_0^2 + 1\right) - (C_{kin} + C_d)C_{kin}R_{kin}^2\omega_0^2 - 1 = C_{kin}^2R_{kin}^2C_dL\omega_0^4 + \left[C_dL - (C_{kin} + C_d)C_{kin}R_{kin}^2\right]\omega_0^2 - 1 = 0. \tag{4}$$

If the parameters of the lumped circuit take finite positive values then Eq. (4), in general, has four (complex) roots. However, since the intercept frequency cannot be complex and must have a positive value, the only relevant solution of Eq. (4) has the following form

$$\omega_0 = \left(\left(\left[\frac{C_dL - (C_{kin} + C_d)C_{kin}R_{kin}^2}{2LC_dC_{kin}^2R_{kin}^2}\right]^2 + \frac{1}{LC_dC_{kin}^2R_{kin}^2}\right)^{0.5} - \frac{C_dL - (C_{kin} + C_d)C_{kin}R_{kin}^2}{2LC_dC_{kin}^2R_{kin}^2}\right)^{0.5}. \tag{5}$$

Eq. (5) shows that ω_0 is a function of R_{kin}. The intercept frequency, $f_0 = \omega_0/(2\pi)$, is plotted as a function of R_{kin} in Fig. 2. f_0 reveals a sigmoid-shaped curve enclosed between two limiting lines. The lower and upper limit, which are shown as dashed lines in Fig. 2, are mathematically derived from Eq. (5) when R_{kin} approaches zero and infinity, respectively. It is generally accepted that R_{kin} reveals an Arrhenius behavior [16,24], which can be given by

$$\frac{1}{R_{kin}} = A\exp\left(-\frac{E_a}{RT}\right) \tag{6}$$

where A is the pre-exponential factor, E_a the activation energy, R the gas constant and T is the absolute temperature. When R_{kin} is substituted in Eq. (5), an expression for f_0 is obtained as a function of temperature. The result is plotted in the insert of Fig. 2 and reveals that a decreasing intercept frequency is theoretically expected at higher temperatures. This makes the intercept frequency suitable for temperature indication of the battery. In the following sections this theoretical statement will be checked experimentally and ready-to-use algorithms will be developed.

3. Experimental

Three batteries have been investigated experimentally: a pristine high power 2.3 Ah $LiFePO_4$ ANR26650 cylindrical battery (A123 Systems), pristine and cycled 7.5 Ah cylindrical ultra-high power $Li(NCA)O_2$ batteries (GAIA Akkumulatorenwerke GMBH). All batteries have graphite anodes. All pristine batteries have been activated by (dis)charging these four times according to the specifications of the manufacturers. Charging and discharging is performed using Maccor automated cycling equipment (Model 4200). The impedances were measured in the galvanostatic mode with an Autolab PGSTAT30 (Metrohm) in the frequency range of 0.01 Hz–30 kHz, using 50 frequencies logarithmically distributed. The current amplitude was set to 200 mA RMS. During all measurements the batteries were located in climate chambers (Maccor, model MTC-010). Measurements were conducted at −20, −10, +10, +30 and +50 °C. Before conducting measurements at a predefined temperature, 3 h of rest have been applied to reach thermal equilibrium. Five SoC values have been investigated, ranging from 100% to 20% in steps of 20%. The intercept frequency has been determined by interpolating the imaginary part of the impedance spectrum to $Z_{im} = 0$.

4. Results and discussion

Fig. 3 shows the Nyquist impedance spectra of a pristine NCA cell at −10 °C and varying SoC. The total impedance varies considerably with SoC, especially the large semicircle in the low frequency region. On the other hand, the small semicircle and the

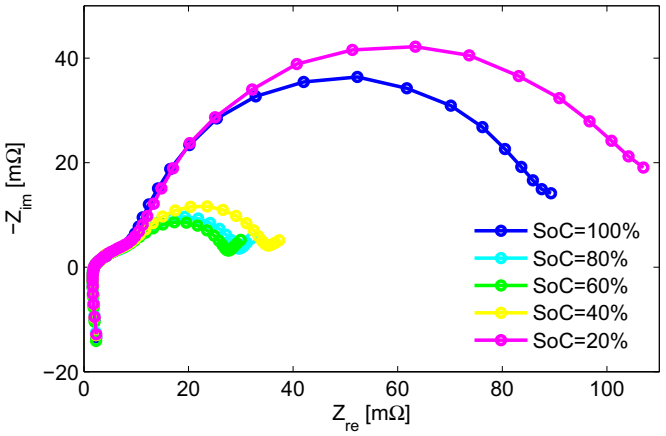

Fig. 3. Impedance spectra of a pristine NCA cell measured at −10 °C and varying SoC.

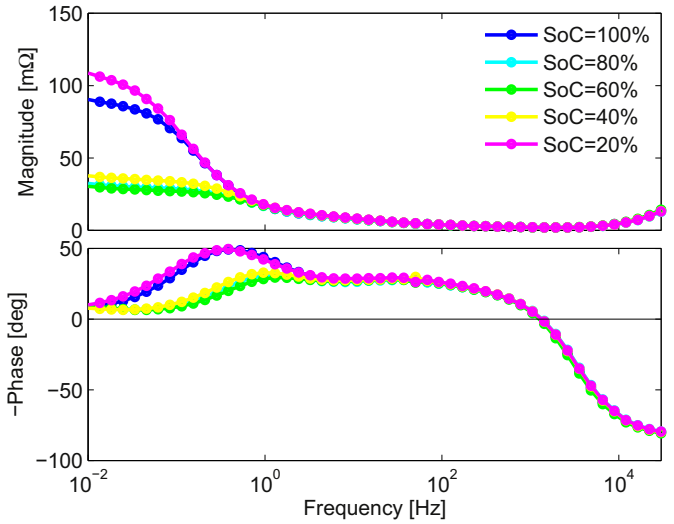

Fig. 4. Impedance results of Fig. 3 represented in a Bode plot.

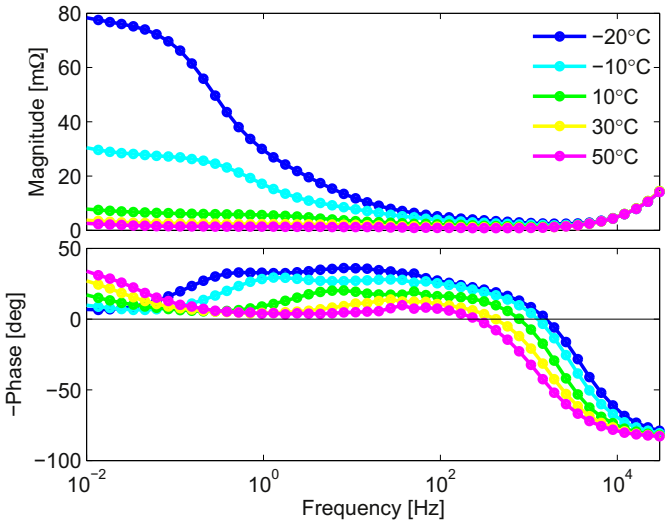

Fig. 6. Impedance results of Fig. 5 represented in a Bode plot.

inductive tail at higher frequencies show only a small dependence on SoC. This becomes more clear in Fig. 4 where the same impedance results are plotted in a Bode diagram. The intercept frequency is the same for all SoC.

Fig. 5 shows the impedance spectra of a pristine NCA cell at 60% SoC at various temperatures. As expected, the large semicircle increases significantly at lower temperatures. It can also be seen that the small semicircle exhibits a similar behavior as the large semicircle and that the whole impedance curve is shifted to the left as the temperature increases, indicating a decreasing ohmic resistance. Furthermore, it can be noticed that the inductive characteristics remain more or less constant. In the Bode plot of Fig. 6 it can be seen that the intercept frequency clearly changes as a function of temperature. It is evident that the intercept frequency decreases with increasing temperature. Plotting the intercept frequency as a function of temperature for a pristine NCA cell (Fig. 7) and $LiFePO_4$ cell (Fig. 8), an exponential behavior is found for both chemistries, which is essentially independent of SoC. These measurement results confirm the theory described in Section 2. The intercept frequencies for the $LiFePO_4$ cell are, however, about five times larger than those of the NCA cell, as can be expected for different sizes and chemistries (see Eq. (5)).

From these results it can be concluded that a similar intercept frequency dependence on the temperature is found to be

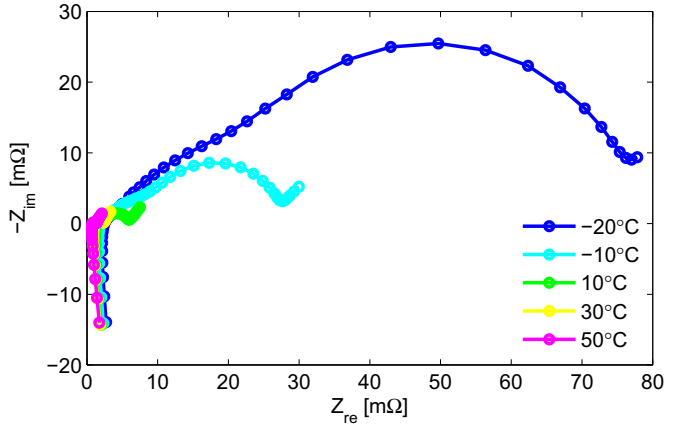

Fig. 5. Impedance spectra of a pristine NCA cell measured at 60% SoC for five different temperatures.

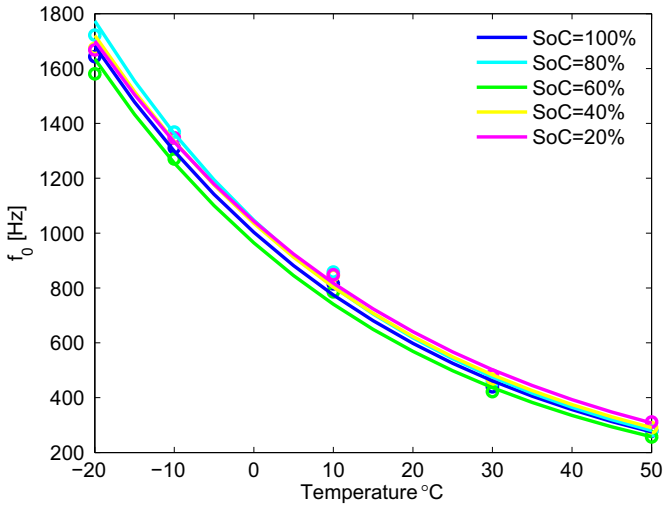

Fig. 7. Intercept frequency as a function of temperature for a pristine NCA cell.

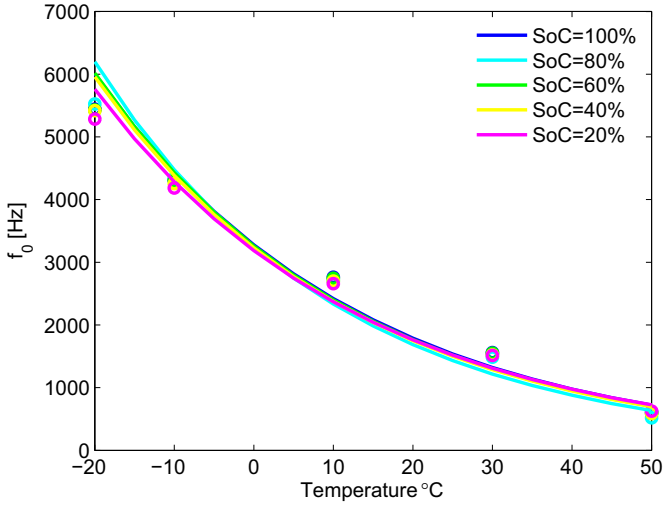

Fig. 8. Intercept frequency as a function of temperature for a $LiFePO_4$ battery.

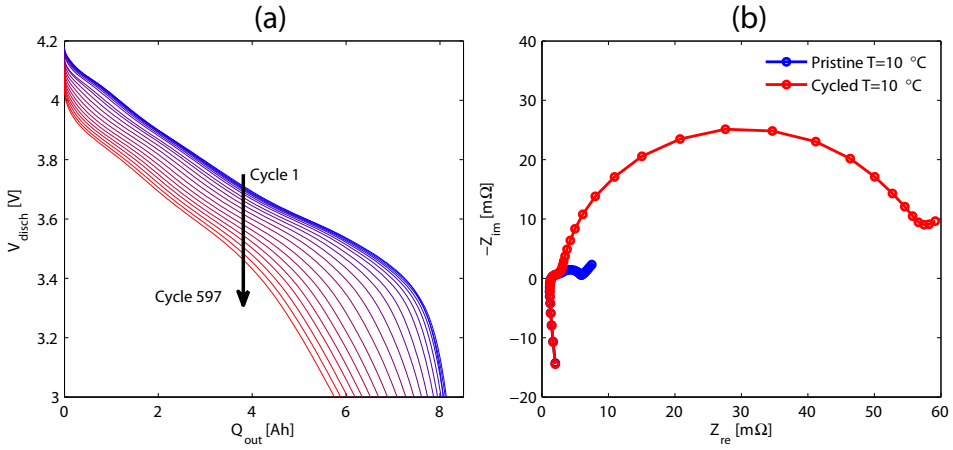

Fig. 9. (a) Voltage discharge curves upon cycling a NCA cell; (b) Impedance spectra of a pristine and cycled NCA cell at 60% SoC and 10 °C.

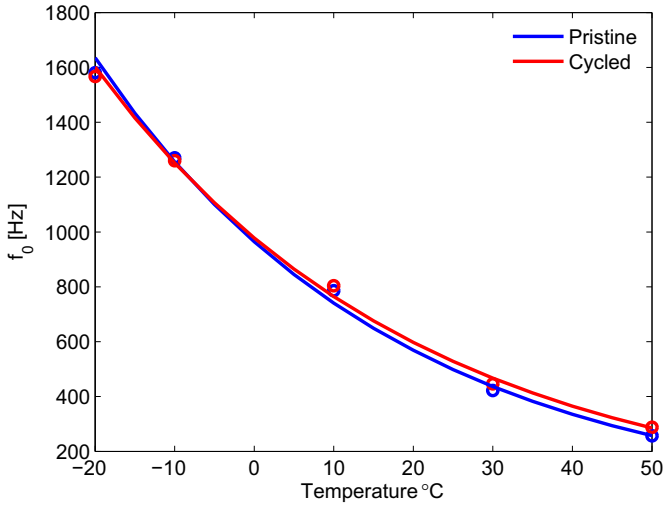

Fig. 10. Measured Intercept frequency as a function of temperature for a pristine and cycled NCA cell at 60% SoC.

independent of battery chemistry, dimension and storage capacity. An interesting question is how battery aging influences the intercept frequency. In order to investigate this, a 7.5 Ah NCA cell has been cycled for about 600 times. Some of the voltage discharge curves are shown in Fig. 9a. About 25% of the storage capacity is lost and the discharge overpotentials are significantly increased after 600 cycles, indicating a major impedance increase. Fig. 9b shows, as an example, the Nyquist plots of the pristine and cycled NCA cell at 10 °C and 60% SoC. In line with the voltage discharge curves (Fig. 9a), it can be seen that the impedance of the cycled cell at low frequencies has dramatically increased. In this particular case there is no significant increase in series resistance, i.e. increase in IR drop. According to Eq. (5) an increase in series resistance, however, should not influence the intercept frequency as a function of temperature, because it is not present in this equation and therefore has no influence on the temperature indication. The spectra at high frequencies did not change upon cycling, indicating that the intercept frequency is independent of aging. This conclusion is confirmed in Fig. 10 where the intercept frequency is plotted as a function of temperature for both the pristine and the cycled cell. This figure proves that the intercept frequency did not change upon cycling.

5. Conclusions

The intercept frequency, i.e. the frequency at which the phase shift between voltage and current is zero, is extracted from impedance spectra of a Li(NCA)O_2 and a $LiFePO_4$ battery and related to the internal battery temperature. A theoretical analysis based on a simple equivalent electrical network model revealed that the intercept frequency is expected to decrease with increasing temperature. Experiments confirmed this finding and additionally showed that the intercept frequency does not depend on SoC. Measurements on a cycled NCA battery showed that the intercept frequency remains stable during cycling. Additional measurements were conducted on 60 Ah $LiFePO_4$ prismatic batteries. These measurements gave results similar to those of the NCA and $LiFePO_4$ batteries. The proposed temperature indication method is therefore readily applicable to batteries of different chemistries, dimensions and storage capacities.

References

[1] S. Gopukumar, D.H. Gregory, H.-S. Kim, D. Shu, Int. J. Electrochem. 2012 (2012) 2.
[2] A. Ritchie, W. Howard, J. Power Sources 162 (2006) 809–812.
[3] B. Scrosati, J. Hassoun, Y.-K. Sun, Energy Environ. Sci. 4 (2011) 3287–3295.
[4] R. Srinivasan, B.G. Carkhuff, M.H. Butler, A.C. Baisden, Electrochim. Acta 56 (2011) 6198–6204.
[5] C. Forgez, D.V. Do, G. Friedrich, M. Morcrette, C. Delacourt, J. Power Sources 195 (2010) 2961–2968.
[6] C.-Y. Lee, S.-J. Lee, M.-S. Tang, P.-C. Chen, Sensors 11 (2011) 9942–9950.
[7] B.V. Ratnakumar, M.C. Smart, S. Surampudia, in: Battery Conference on Applications and Advances, 2002. The Seventeenth Annual, 2002, pp. 273–277.
[8] M. Mohamedi, H. Ishikawa, I. Uchida, J. Appl. Electrochem. 34 (2004) 1103–1112.
[9] D. Andre, M. Meiler, K. Steiner, C. Wimmer, T. Soczka-Guth, D.U. Sauer, J. Power Sources 196 (2011) 5334–5341.
[10] J. Li, E. Murphy, J. Winnick, P.A. Kohl, J. Power Sources 102 (2001) 294–301.
[11] M.D. Levi, K. Gamolsky, D. Aurbach, U. Heider, R. Oesten, Electrochim. Acta 45 (2000) 1781–1789.
[12] S. Rodrigues, N. Munichandraiah, A.K. Shukla, J. Solid State Electrochem. 3 (1999) 397–405.
[13] T. Momma, M. Matsunaga, D. Mukoyama, T. Osaka, J. Power Sources 216 (2012) 304–307.
[14] P. Suresh, A.K. Shukla, N. Munichandraiah, J. Appl. Electrochem. 32 (2002) 267–273.
[15] S.S. Zhang, K. Xu, T.R. Jow, Electrochim. Acta 49 (2004) 1057–1061.
[16] L. Liao, P. Zuo, Y. Ma, X. Chen, Y. An, Y. Gao, G. Yin, Electrochim. Acta 60 (2012) 269–273.
[17] X.-Y. Qiu, Q.-C. Zhuang, Q.-Q. Zhang, R. Cao, P.-Z. Ying, Y.-H. Qiang, S.-G. Sun, Phys. Chem. Chem. Phys. 14 (2012) 2617–2630.
[18] J. Gomez, R. Nelson, E.E. Kalu, M.H. Weatherspoon, J.P. Zheng, J. Power Sources 196 (2011) 4826–4831.
[19] N.A. Hampson, S.A.G.R. Karunathilake, R. Leek, J. Appl. Electrochem. 10 (1980) 8.

[20] F.C. Laman, M.W. Matsen, J.A.R. Stiles, J. Electrochem. Soc. 133 (1986) 2441–2446.
[21] J.Y. Song, H.H. Lee, Y.Y. Wang, C.C. Wan, J. Power Sources 111 (2002) 255–267.
[22] E. Karden, Ph.D. Dissertation, RWTH Aachen, Germany, Aachen, 2001.
[23] B. Savovastoynov, Z.B. Stoynov, J. Appl. Electrochem. 17 (1987) 1150–1158.
[24] W. Waag, S. Kaebitz, D.U. Sauer, Appl. Energy 102 (2013) 885–897.
[25] Y. Zhang, C.-Y. Wang, J. Electrochem. Soc. 156 (2009) A527–A535.
[26] J.P.M. van Lammeren, M.J.G. Lammers, L.H.J. Raijmakers, D. Danilov, P.H.L. Notten, in: Fachtagung Kraftwerk Batterie, Aachen, Germany, 2013.